



TOTEM Results and Perspectives for 2010/2011

The TOTEM Collaboration

Abstract

The status of the TOTEM experiment and the plans for the installation of the T1 detectors are presented. First preliminary results about large $|t|$ elastic proton scattering are discussed. Proposed future running scenarios will extend the measurement of elastic scattering to smaller $|t|$ -values and also allow precise measurements of event topologies with the forward tracking detectors. The commissioning of large β^* optics is a necessity for the total cross-section measurement next year.

1 Introduction

It is the primary goal of TOTEM [1, 2] to measure the total cross-section in a luminosity independent way. This requires a precise measurement of elastic scattering at small momentum transfers ($|t| \sim 10^{-3}$ to 10^{-1} GeV²) to enable an extrapolation to the Optical Point at $t = 0$, and a careful study of diffraction (single and double diffraction and double Pomeron exchange) which accounts together for 25 – 40% of the inelastic cross-section. The elastic scattering measurement at these low $|t|$ -values will need a special beam optics with $\beta^* = 90$ m or larger to keep the angular spread of the beam much smaller than the scattering angle. Presently, TOTEM runs in parallel with the other experiments at a β^* of 3.5 m. This allows measurements of the elastic scattering at larger $|t|$ -values (presented in the next chapter) and first studies of diffraction using only the protons in the RP detectors. The forward GEM gas detectors ($5.3 < \eta < 6.5$) were also used actively in the trigger to obtain first multiplicity distributions in the forward regions. However, final results on event topologies can only be expected when TOTEM will run at lower luminosities per bunch to avoid pile-up events.

2 Recent Results and Experience

2.1 First Measurements of Elastic Scattering

The Roman Pot (RP) detectors have been fully installed at the 220 m location on both sides of the Intersection Point IP5 (Fig. 1). One unit consists of two vertical and one horizontal pot together with a beam position monitor (BPM). Two units separated by 5 m form a powerful spectrometer with an excellent position resolution (typically $40 \mu\text{m}$ including alignment imperfections) and angular resolution (typically $10 \mu\text{rad}$).

The precise alignment of the RP detectors with respect to each other and to the beam is vital. Tracks passing through the overlap of the vertical and horizontal detectors are used for the internal alignment of the RP detectors, whereas the alignment of the RPs w.r.t. the beam takes advantage of the sharp edge of the proton beam created by the LHC collimator system during special collimator/RP setup runs. For the vertical alignment the distribution of the diffractive protons in the horizontal detectors is used. Furthermore, the well-defined and constrained elastic scattering events will be used for a precise alignment of the spectrometers.



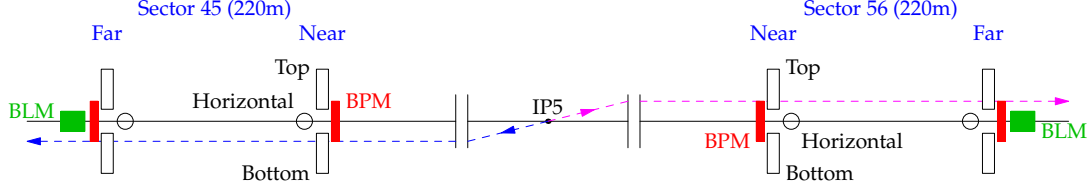
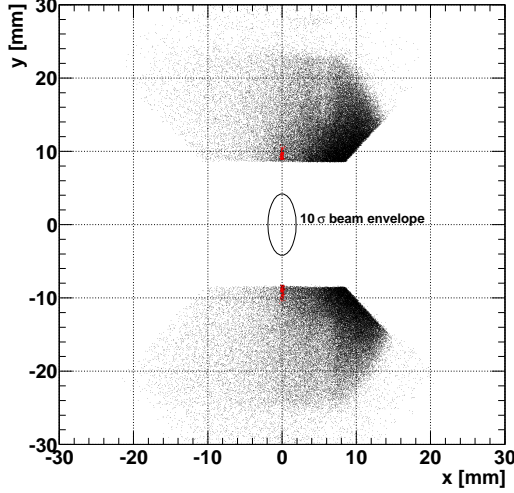


Figure 1: *Schematic view of the Roman Pot system presently installed.*



$$\begin{aligned} y(s) &= v_y(\xi, s) \cdot y^* + L_y(\xi, s) \cdot \Theta_y^* \\ x(s) &= v_x(\xi, s) \cdot x^* + L_x(\xi, s) \cdot \Theta_x^* + \xi \cdot D(\xi, s) \end{aligned} \quad (1)$$

with

$$\begin{aligned} v(\xi, s) &= \sqrt{\frac{\beta(\xi, s)}{\beta^*}} \cos \Delta\mu(\xi, s) \\ L(\xi, s) &= \sqrt{\beta(\xi, s)\beta^*} \sin \Delta\mu(\xi, s) \\ \Delta\mu(\xi, s) &= \int_0^s \frac{1}{\beta(\xi, s')} ds' \end{aligned} \quad (2)$$

Figure 2: *Left: Distribution of track intercepts in the central planes of the RP220 stations (i.e. in the middle between the near and far units) in sector 4-5 (bottom) and 5-6 (top). The red points correspond to the elastic events. Right: Equations describing the transverse track trajectories as a function of the longitudinal orbit coordinate s , and the definitions of the optical functions.*

About two million events, corresponding to an integrated luminosity of 80 nb^{-1} , have been taken with a coincidence trigger between the vertical RP detectors in the two arms (see Fig. 1). To search for collinear elastic scattering events, a track in the top of side (5-6) and in the bottom of side (4-5) passing through the near and the far detectors was required, leaving about 60 kevents. The distribution of these tracks over the top and the bottom detectors, which are placed symmetrically at about $8.5 \text{ mm} \approx 20\sigma$ from the beam centre (Fig. 2), show at least three distinct regions: the $x < 0$ side is mainly populated by the background like e.g. beam halo, whereas the diffractive protons are shifted to the $x > 0$ side due to their momentum loss by $\Delta x = D\xi$ (cf. Eqn. (1)) where $\xi = \frac{\Delta p}{p}$ ($D < 0$ is the dispersion and due to $\xi < 0$ acts in the positive x direction). The elastic scattering events (red points in Fig. 2) are distributed in a very narrow band around $x = 0$. The transverse positions of the protons in x and y are given by the optical functions (Eqn. (2)) which depend on the momentum loss ξ of the protons due to chromaticity effects. For example, L_y changes from $+20 \text{ m}$ at $\xi = 0$ to -40 m at $\xi = -0.1$ (corresponding to a horizontal position $x = 10 \text{ mm}$).

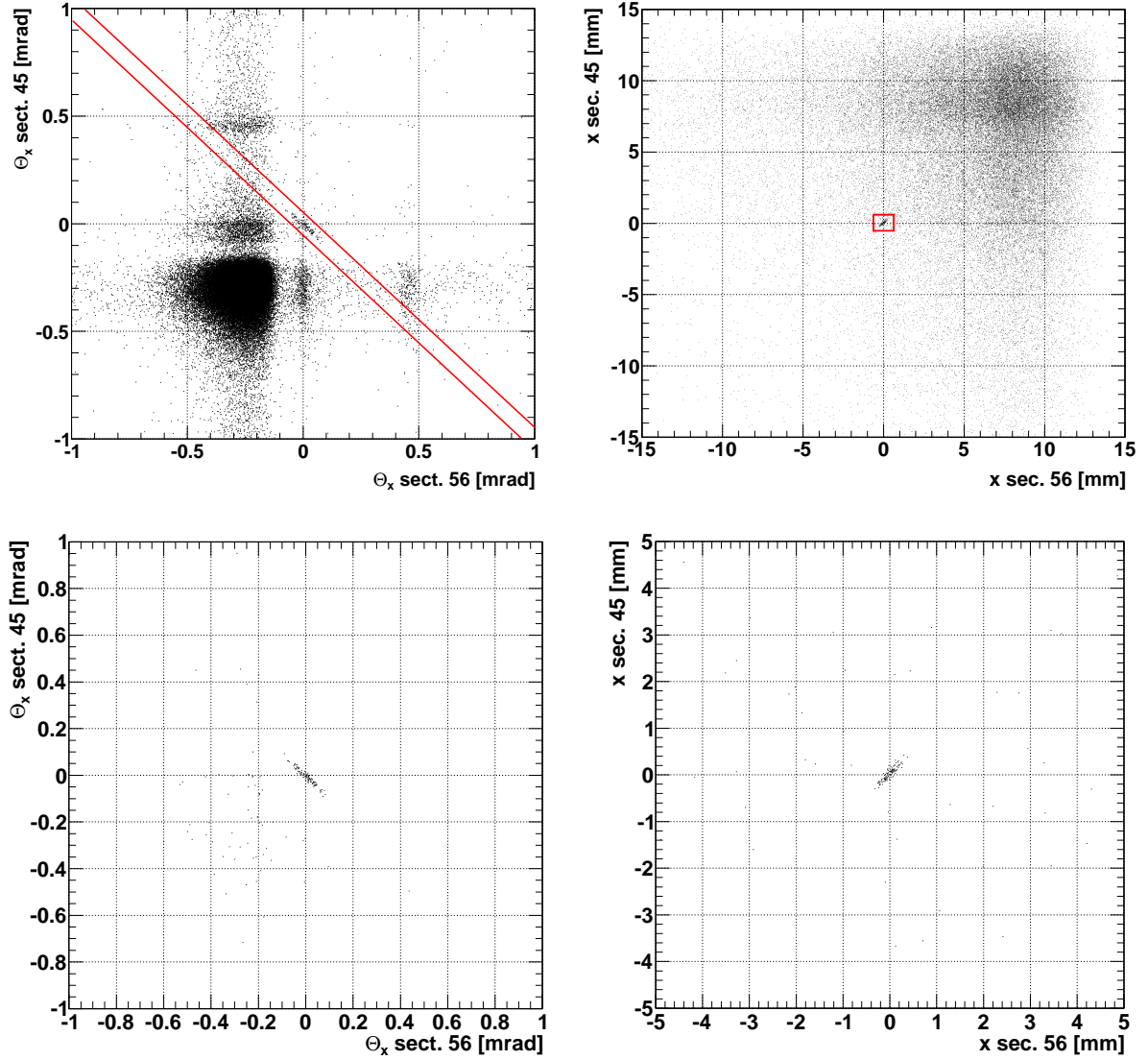


Figure 3: *Top: correlation of the local horizontal track angles Θ_x (left panel) and of the x positions in the longitudinal station centres (right panel) between the RP system arms in sectors (4-5) and (5-6) for all events selected for Fig. 2. Bottom: same correlations as in the top panels but with an x -position cut for the angular correlation (left), and with an angular cut for the position correlation (right). These cuts are shown in the top panels.*

The selection of elastic events in this first analysis is mainly based on the angle Θ_x and the x position measured in the spectrometers on both sides. The angle Θ_x is related to the scattering angle Θ_x^* in the IP by

$$\Theta_x = \frac{dL}{ds} \Theta_x^*. \quad (3)$$

Figs. 3 (top left and top right) show the scatter plots (left arm versus right arm) of the angular and the position measurements of the selected events displayed in Fig. 2. The expected angular correlation near the origin is already clearly visible without applying any cuts. The accumulation at the zero position is hardly visible but becomes significant in Fig. 3 (bottom, right), where the events are selected around the diagonal of Fig. 3 (top, left) within a band of ± 0.0385 mrad. Vice versa (Fig. 3 bottom left) the angular

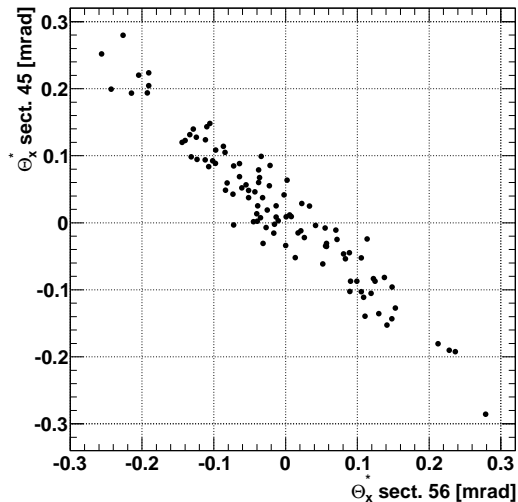


Figure 4: Correlation of the horizontal scattering angles Θ_x^* between the RP system arms in sectors (4-5) and (5-6) for the final event sample, i.e. after the position and angle cuts shown in the top panels of Fig. 3.

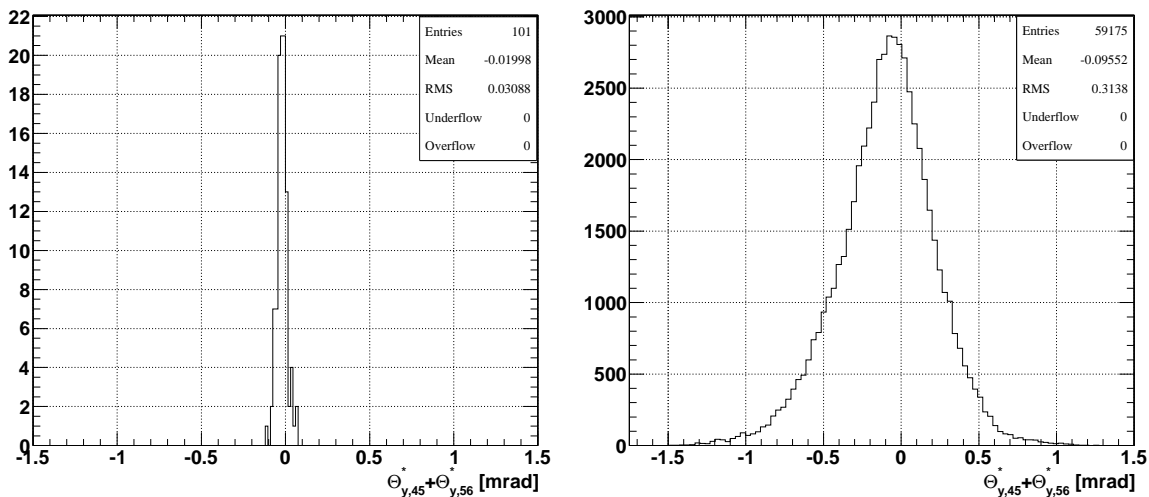


Figure 5: Difference between the scattering angles Θ_y^* reconstructed independently in both arms for the elastic candidate events (left) and all events (right).

correlation is further cleaned by an x-position cut around zero (corresponding to ξ close to 0) with a tolerance of ± 0.6 mm. Applying cuts in both position and angle yields a highly refined, almost background free, event sample of elastic candidates which exhibits a strong correlation of the scattering angles between the two forward arms as expected for a collinear scattering process (Fig. 4).

The orthogonal y-projection is independent of the x-direction in which the candidate events were selected. The difference between the scattering angles Θ_y^* reconstructed independently in both arms is shown in Fig. 5 (left) for the selected elastic candidate events, to be compared with the same plot for the full sample of 60 k events (Fig. 5, right). The striking difference between the two distributions demonstrates the strong angular correlation in the elastic candidate events. The collinearity requirement in the y-projection within the systematic error limits determined the final definition of the elastic event sample.

Double Pomeron Exchange (DPE) or pile-up of SD events are a potential background to elastic scattering. Exploiting the measurements of top-top or bottom-bottom double-arm coincidences, it is possible to quantify and subtract this background.

Finally, the t -distribution of the elastic data sample is compared with the Monte-Carlo using three models [3] normalised to the integrated luminosity of the data (Fig. 6). The detector and the optics have been fully simulated. At this preliminary stage of the analysis, the data appear to be compatible with the two first models of Ref. [3] (which cannot be distinguished with the present limited statistics). Also the third model cannot be excluded because a shift of the detector positions by 1σ can change the rate by a factor 2.

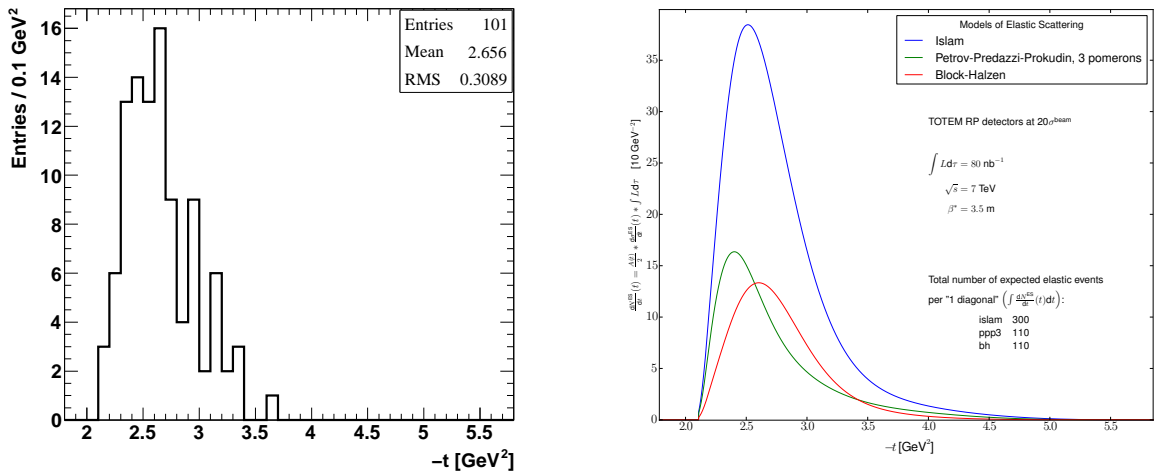


Figure 6: *Left: preliminary reconstructed $|t|$ -distribution. Right: simulated $|t|$ -distribution according to three models [3], with full event reconstruction but without any resolution effects.*

These data correspond to three hours of data taking with the detectors at a distance of about 20σ from the beam centre. Longer runs at a distance of 15σ will lower the $|t|$ -threshold and increase the statistics considerably. This will allow a better comparison with the models and will enable TOTEM to carefully check the optics of the LHC machine.

2.2 T2 Detector Performance and Physics

2.2.1 Optimisation studies

The optimisation of the detector has followed two different lines. The first one consisted in searching for the hardware biases that could decrease the detector efficiency; the second one was to review the cluster and tracking algorithms in order to enhance the performance of the track reconstruction.

Hardware (buffer latencies, thresholds)

A list of dead channels has been established, containing 8% of all the T2 channels. About 1% of them were already present before the installation in IP5, due to VFAT chips with a broken connection on the 11th card.¹ In addition, the cables connecting the detectors

¹The data of each VFAT are sent serially to the DAQ. If the connection is broken, all 128 channels are lost.

and the optical transmitter boards have been damaged during the installation; the last installed detector suffered the most. This problem will be partially fixed if we have the opportunity to change the damaged cables during the winter shutdown. Fortunately, due to the large redundancy in the number of planes, the tracking efficiency is only marginally affected by this problem.

The handles we have to optimise the detector performance are the detector gain, the discriminator threshold and the front-end chip latency optimisation. We made scans in gain with fixed thresholds. Little increases were needed to reach the plateau. The tests showed that the best results were obtained by keeping the thresholds with a safe margin to the noise and doubling the chamber gain. The latency scans instead revealed a more complicated pattern, and the wrong timing was causing most of the detector inefficiencies. Three out of four quarters were a few clock cycles away from the optimum latency, causing a significant drop of the hit efficiency. The new parameters increased the hit efficiency close to the expected value.

Software (cluster and track algorithms)

The original tracking algorithm required geometrically overlapping pad and strip clusters to define a hit for the track reconstruction. Thus some valid pad and strip hits were excluded from the track fits. In the updated algorithm separate pad and strip clusters can be associated to a track. This led to an increase of the efficiency, in particular in the regions where either pad or strip VFAT information is missing due to the aforementioned hardware problems.

2.2.2 Efficiency (Pad and strip intrinsic efficiency, track efficiency)

Fig. 7 shows the hit efficiency of the detectors calculated by using the tracks from the latest physics runs. While for the pads the efficiencies are reaching the expected level, still the cluster definition and some cross-talk induced noise jumps of strip groups affect the strip efficiency of some detectors. The work is still in progress although the present algorithm already allows a very good tracking efficiency.

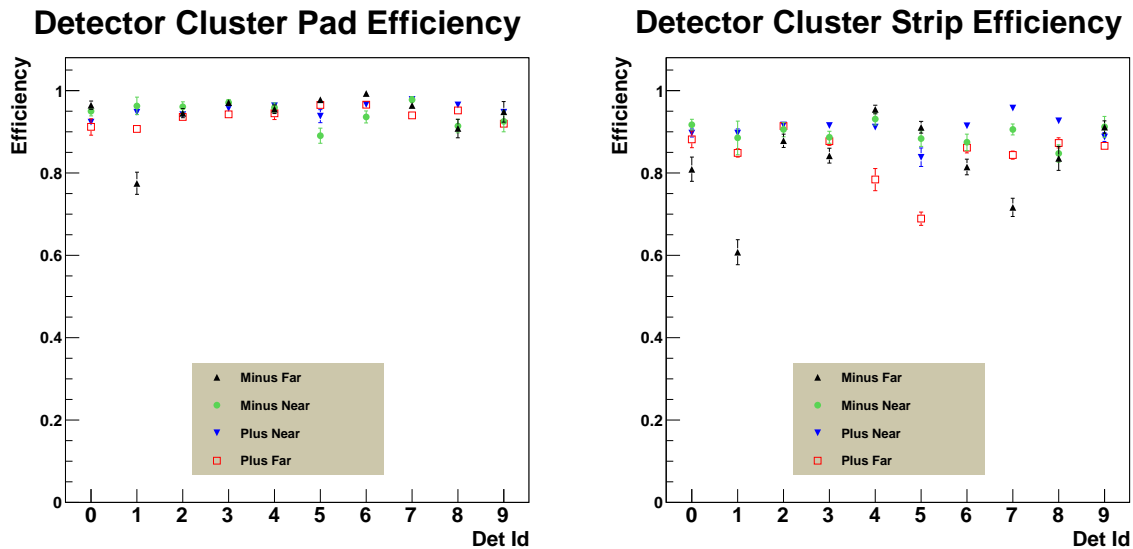


Figure 7: *Efficiency of the T2 pads (left) and strips (right).*

2.2.3 Pseudo-Rapidity Resolution

The intrinsic η -resolution of the detector has been estimated from the spread of the η -values obtained by connecting the ideal vertex with the individual track hits (Fig. 8). For the good tracks pointing to the vertex the fit was constrained to include the vertex position. These measurements are compared to Monte-Carlo reconstructed tracks fitted including the vertex. The data shown here are in a good agreement with the pure geometrical resolution.

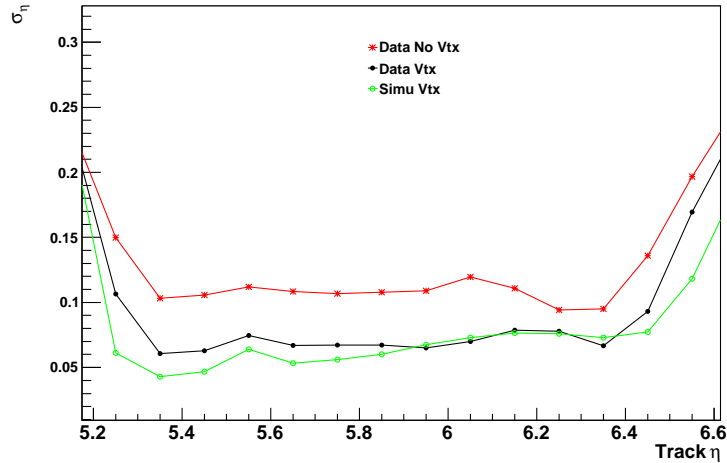


Figure 8: *Simulated and measured resolution in η .*

2.2.4 Measurement of the Pseudo-Rapidity Distribution

The $dN/d\eta$ distribution (Fig. 9) – previously presented in [4] – has been recalculated for the same data from early runs with low luminosity per bunch crossing, where the pile-up of proton interactions was negligible. The new tracking algorithms were used. Compared to the old result, the mean number of tracks shows an increase due to a better track reconstruction. The systematics related to the contamination from secondary particles is currently under evaluation, though we expect that the primary vertex requirements for the reconstructed tracks would reduce significantly their contribution.

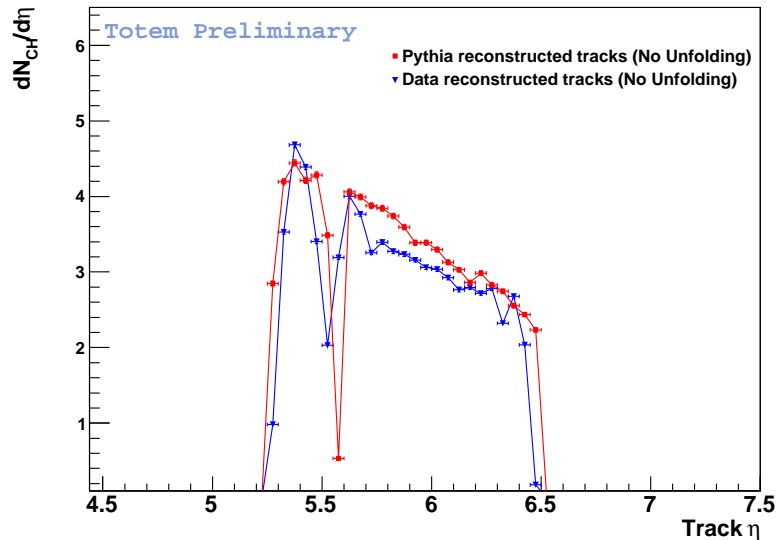


Figure 9: *Simulated and measured pseudo-rapidity distribution. The dip at $\eta \approx 5.5$ is caused by interactions in the transition between two different beam pipe sections.*

3 Installation of T1

3.1 Physics Motivation of the T1 Installation

As seen in Fig. 9, the T2 tracker covers the η region between 5.3 and 6.5 with a loss around 5.5 due to particle interactions. The acceptance is considerably increased once T1 – covering $3.1 \leq |\eta| \leq 4.7$ – is installed. As shown in Table 1, maximal $|\eta|$ coverage is required to minimise the systematic uncertainty of the measurement of the inelastic rate. Having the full T1 detector installed will enable the selection of pure single (SD) and double diffractive (DD) event samples using the event topologies as reconstructed in the T1 and T2 telescopes. The measurement of the individual rates of all diffractive processes at a 5 – 10% level can then be used as a consistency check for the overall inelastic rate and makes an extrapolation of the individual cross-sections possible.

For an estimate of the inelastic rate uncertainties for the different detector configurations, the PYTHIA generator [8] was used for the description of the non-diffractive minimum bias (MB) events, whereas PHOJET [7] was preferred for describing diffraction. Based on Refs. [5, 6, 7, 8], the MB cross-section at $\sqrt{s} = 7$ TeV is predicted to be 40 – 60 mb, and the SD and the DD cross-sections to be 10 – 15 mb and 4 – 11 mb, respectively. For the rate estimates, the central values of the predicted cross-section ranges have been used, and for the uncertainty estimates, the cross-sections have been allowed to vary over the indicated ranges. The systematic uncertainties were estimated by treating the same initial inelastic event sample once with a tight event selection and once with a looser selection – based on the number of reconstructed tracks – and comparing the resulting inelastic rates.

	MB			DD			SD		
	T1+T2	1/2 T1 + T2	T2 only	T1+T2	1/2 T1 + T2	T2 only	T1+T2	1/2 T1 + T2	T2 only
1(L+R)	100.0%	100.0%	98.2%	94.1%	92.9%	89.8%	77.6%	75.4%	71.3%
2(L+R)	100.0%	99.5%	95.1%	88.9%	83.4%	73.8%	68.6%	61.9%	51.3%
3(L+R)	99.9%	98.1%	89.0%	83.9%	75.3%	57.5%	61.4%	49.9%	32.3%
4(L+R)	99.1%	95.9%	82.2%	78.2%	66.3%	45.5%	55.0%	40.0%	19.0%
5(L+R)	98.3%	93.2%	71.7%	73.3%	59.5%	33.3%	48.4%	31.4%	11.5%

Table 1: *Fraction of events reconstructed for non-diffractive minimum bias (MB), double diffraction (DD) and single diffraction (SD) for different detector configurations with one (“1(L+R)”), two (“2(L+R)”), etc. charged tracks pointing to the interaction point.*

From Table 1 it can be seen that the fraction of lost events, in particular the diffractive component, is substantially reduced going from the (T2 + 1/2 T1) configuration to the (T2 + full T1) configuration independently of the inelastic event selection. A minimum of 3 tracks per event seems to be realistic for a clean event definition.

The availability of both T1 arms for the inelastic rate measurement will minimise the following uncertainties:

- The large uncertainties of the particle distributions of inelastic processes at large $|\eta|$ will inevitably lead to uncertainties in the fraction of accepted events. The larger the fraction of accepted events is, the smaller the uncertainty in the extrapolated inelastic rates will be.
- The cross-section of low-mass diffractive events, in which all particles are produced at $|\eta|$ -values beyond the T2 acceptance, is estimated to be 2.9 mb. The procedure to correct for this loss is based on an extrapolation of the acceptance-corrected

	T2 + full T1	T2 + 1/2 T1	T2 only
Total loss requiring 3 particles	6.1 mb	9.1 mb	17.1 mb
Uncertainty on event description	0.81 mb	1.6 mb	3.8 mb
Uncertainty on low mass diffraction estimate	0.60 mb	1.2 mb	1.9 mb
Total (relative) uncertainty	1.0 mb (1.4 %)	2.0 mb (2.9 %)	4.3 mb (6.1 %)

Table 2: *Top line: estimated total loss requiring 3 charged particle pointing to the interaction point in inelastic event selection. Second and third line: dominant contributions to the uncertainty of the rate measurement and their dependence on the detector configuration. Bottom line: total (relative) uncertainty.*

diffractive distribution from Monte Carlo [1, 2]. Experimentally, this extrapolation is driven by events with low diffractive masses ($M < 100$ GeV), i.e. events where the particles from the decay of the diffractive system are emitted exclusively in one hemisphere. The uncertainty of this procedure depends on the purity of the reconstructed diffractive sample used for the extrapolation. This purity increases from about 60% for the (T2 + 1/2 T1) configuration to above 90% for (T2 + full T1) due to a significant decrease of the number of MB events reconstructed as having charged particles only in one hemisphere and thus mis-identified as SD events.

For the realistic case of 3 required tracks to define an inelastic event, Table 2 summarises the total lost cross-section with the main uncertainties arising from the event topology and the extrapolation to low-mass diffraction.

The final (relative) uncertainty on the inelastic cross-section measurement at $\sqrt{s} = 7$ TeV is estimated to be 1.0 mb (1.4%), 2.0 mb (2.9%) and 4.3 mb (6.1%) in the case of the (T2 + full T1), (T2 + 1/2 T1) and (T2 only) configurations, respectively.

The cross-section measurement at 7 TeV will also provide a determination of the luminosity independent of the methods applied by the machine.

3.2 T1 Detector Performance

The four half-arms of the T1 telescope, equipped with all CSCs, read-out electronics and services, have been installed on the SPS test beam line H8 in the North Area (Fig. 10). Extensive tests have been conducted in different running periods in autumn 2009 and spring-summer 2010, with one of the two arms alternately connected to the power supplies and the data acquisition system.

Thresholds and latency values have been tuned after dedicated scans. The optimal latency settings are identical on all half-arms, when the time of flight of beam particles is taken into account. For most of the runs a signal stretching of 3 clock cycles has been used, suitable for data acquisition with an LHC beam interaction period of 75 ns.

Data have been taken with both a pion beam interacting with a Cu target (in position roughly corresponding to the interaction point in CMS with respect to one of the two arms), and with a muon beam crossing all layers of a given sextant.

Hit reconstruction required the coincidence of a wire cluster and two strip clusters, one in each of the two projections measured in the chamber. Track reconstruction required hits in at least 4 CSC layers. An event from a pion beam run on the “second” arm, rendered with the FROG event display, is shown in Fig. 11.

Interaction vertices have been reconstructed in multi-track events resulting from pion scattering on the target. The distributions of the vertex coordinates in a run with the

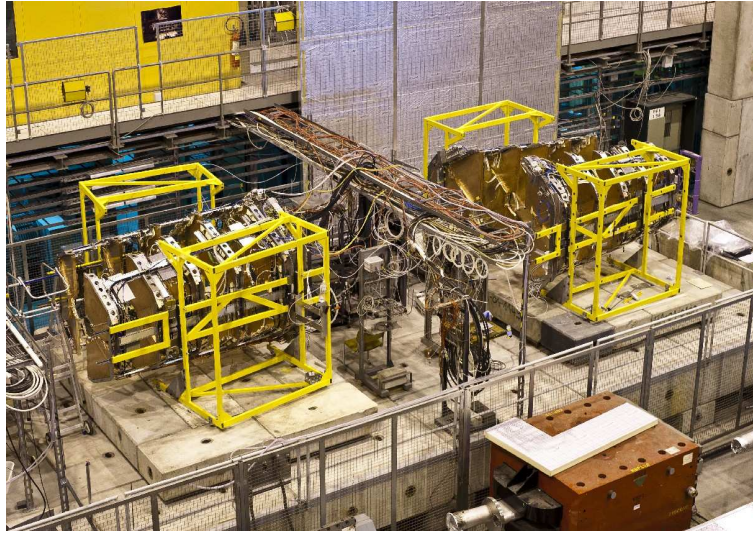


Figure 10: *The two arms of the T1 telescope, back to back on the H8 test beam line.*

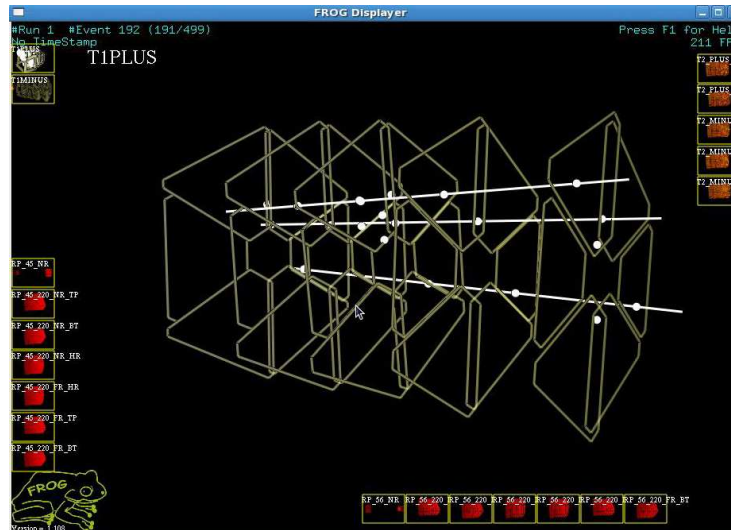


Figure 11: *Reconstructed hits and tracks in an event recorded during a pion run, as seen in the FROG event display. Note the tracks pointing “backwards” because of the inverted orientation of the “second” arm with respect to the target.*

“first” arm is shown in Fig. 12: vertices are centred around the target location, with radial and longitudinal standard deviations of about 3 cm and 85 cm, respectively (with no alignment). Muon runs have been used for a simple determination of the efficiency of chambers in the beam line. Values measured on the “first” arm as a function of the HV applied are shown in Fig. 13 and are, as expected, approaching 100% around 3.45 kV.

During the tests in 2010 all chambers were equipped with the additional protection stage mounted on the anode front-end cards. No damage on the VFAT chips due to occasional sparks has been observed since.

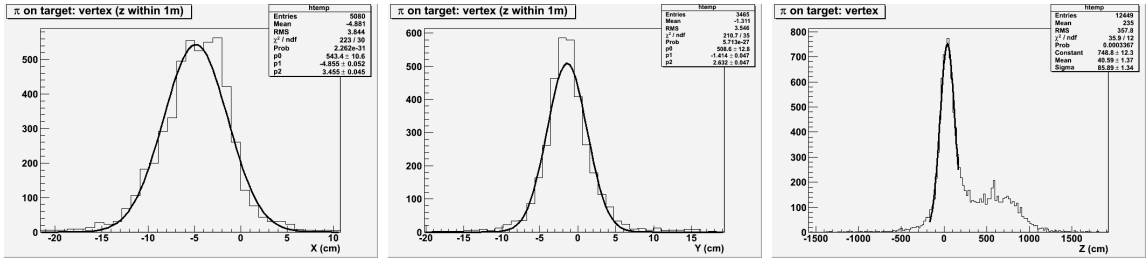


Figure 12: *Distributions of the three coordinates of vertices reconstructed from pion test beam data.*

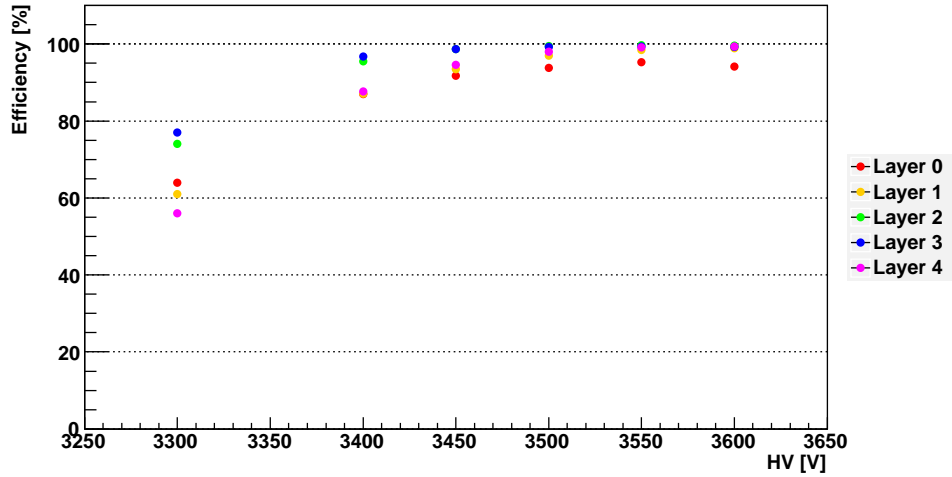


Figure 13: *Hit reconstruction efficiency (using 3-coordinate coincidences) in the CSC of one sextant as a function of applied HV, from muon test beam data.*

3.3 Installation Schedule and Collaboration with CMS

The TOTEM T1 detector system is composed of 4 quarter elements. On each side of CMS – in the following referred to as plus (+) and minus (–) side, two quarter elements will be installed in the conical-shaped volumes, created by the three CMS end cap disks. The installation of the T1 detector within CMS requires several preparatory work processes like the lowering of the CMS-HF, a delicate operation since it will be performed in the proximity of the LHC beam pipe.

In view of the integration of the T1 detector in the CMS experiment, an Engineering Design Review (EDR) was held at CERN on Thursday 24 June 2010 [9]. The scope of the EDR was to review the TOTEM T1 installation procedure and installation-specific tooling, paying attention to integration issues. Underlying logistic requirements and intended quality assurance/control measures such as pre- and post- installation testing were also addressed. Special attention was given to possible risks for the TOTEM or CMS detectors and possible interferences with other activities. Furthermore, all issues related to the time schedule were addressed in detail, as the installation is foreseen in the very limited time window of the end-of-year technical stop 2010-2011. As the installation of the T1(+) side is independent of the T1(–) side, a split in two separate installation work packages for

each side was made. The final schedule however pursues the objective to install both, the T1(+) side and T1(-) side during this upcoming technical stop.

Within the framework of this EDR, an ESR (Electronic System Review) was organised to address issues related to the electrical safety.

Following the EDR, the CMS Technical Coordinator wrote a close-out report [9], summarising the committee's remarks and recommendations. Accordingly, several activities started and were organised in related work packages. The progress of these different work packages is continuously monitored.

CMS and TOTEM are convinced that, following the agreements and recommendations outlined in the EDR close-out report, the successful installation of the T1 detector can be performed in the next shutdown.

4 Plans for 2010/2011

4.1 Data Taking at Standard $\beta^* = 3.5$ m

The elastic data were taken with an asymmetric set of Roman Pot positions which were obtained by extrapolating the calibration from a Roman Pot collimator setup run, taken at 450 GeV per beam, to the physics running energy of 3.5 TeV per beam. One diagonal left-right combination of the vertical detectors was set at approximately 20σ distance to the beam centre, the other one was around 25σ . This can be concluded from Fig. 14 where the y positions (one arm versus the other) for elastic events are shown for the left-bottom / right-top and left-top / right-bottom combinations. The distance to the beam is very critical: an increase of only 2 mm ($\sim 4\sigma$) reduces the elastic rate by a factor 10. In agreement with the collimation group, a new calibration at the nominal beam energy of 3.5 TeV will be performed soon. In this exercise the RP detectors will be driven to the sharp edges of the beams created at about 5σ by the collimators. At the moment when the Beam Loss Monitors downstream of the RPs (see Fig. 1) record a spike in the dose rate, the RPs touch the beam edge, i.e. they are at the same number of beam sigmas as the collimators which have created the edge. TOTEM wants to use this special configuration with a uniquely close beam approach to take data for a few hours.

During standard runs the RP detectors cannot be moved closer than 15σ to the beams to stay in the shadow of the tertiary collimators. However, the machine group has estimated that below 4×10^{10} protons per bunch the risk of damage caused by such a low-intensity beam is low. To approach closer to the beams, TOTEM is therefore interested in taking data in a special run of about 5 hours with $2 - 4 \times 10^{10}$ protons per bunch. The set-up of such a beam is standard except that the beam instrumentation thresholds have to be lowered. During such a short run, TOTEM can take enough data to study the large cross-section phenomena, like elastic scattering and diffraction, under conditions which allow to approach the beams quite close and with a reduced pile-up in the order of a few percent. At high luminosity runs a considerable event pile-up with $2 - 3$ interactions per bunch crossing is produced. Our forward gas detectors cannot resolve this pile-up, and hence TOTEM would like to explore the possibility to add a low-intensity bunch to the usual high-intensity bunch train. This would allow continuous data taking during normal runs without suffering from the pile-up.

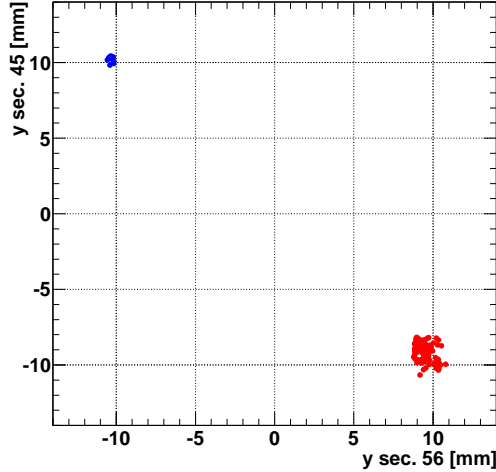


Figure 14: Correlation between the vertical track positions in the RP stations in the left arm (sector 4-5) and the right arm (sector 5-6). The red points correspond to the 20σ diagonal combination (left-bottom / right-top); the blue points correspond to the 25σ combination (left-top / right-bottom).

4.2 Optics with Larger β^*

4.2.1 Acceptance for Elastic Scattering at Small Momentum Transfers

For measurements of elastic scattering at small momentum transfers – particularly in view of differential rate extrapolations to $t = 0$ as an ingredient for the total cross-section measurement – special optics with β^* larger than the injection value of 11 m are needed. This section will focus on the two optics with $\beta^* = 90$ m and $\beta^* = 1540$ m, and compare their acceptances at $\sqrt{s} = 7$ TeV and 14 TeV (see Fig. 15). Note that the expectations for $\beta^* = 1540$ m at 7 TeV have been obtained by rescaling the properties at 14 TeV, while the technical realisation of a very-high β^* optics at this lower energy is still under study (see Section 4.2.4).

The small- $|t|$ limit of the detector acceptance $A(t)$ for elastically scattered protons can be characterised by the value t_{50} at which $A = 50\%$, which is 2 times the minimum reachable value t_{min} (where A becomes 0). For a beam energy $p = \frac{1}{2}\sqrt{s}$ and a detector-beam distance of K times the beam width σ , this figure of merit is given by

$$|t_{50}| = \frac{2p^2}{L_{\text{eff},y}^2} \left(K \sqrt{\frac{\varepsilon_n \beta_y}{\gamma}} + \delta \right)^2 = 5.9 \times 10^{-4} \text{ GeV}^2, \quad (4)$$

where L_y is the effective length in the vertical plane, β_y is the betatron function at the detector, $\gamma = \frac{p}{m_p}$, and $\delta = 0.5$ mm is the distance of the sensitive detector volume from the pot's outer window surface. Fig. 16 (left) shows t_{50} for the $\beta^* = 90$ m and the $\beta^* = 1540$ m optics.

The figure illustrates the two strategies for reaching smaller $|t|$ -values:

- Move the Roman Pot detectors closer to the beam. For small bunch populations ($N \sim 2 \times 10^{10}$) a distance of 10σ or smaller could be achieved.
- Go to lower \sqrt{s} . According to (4), $|t_{50}|$ decreases with reduced proton energy p , but the quadratic dependence due to the leading factor p^2 is weakened by the

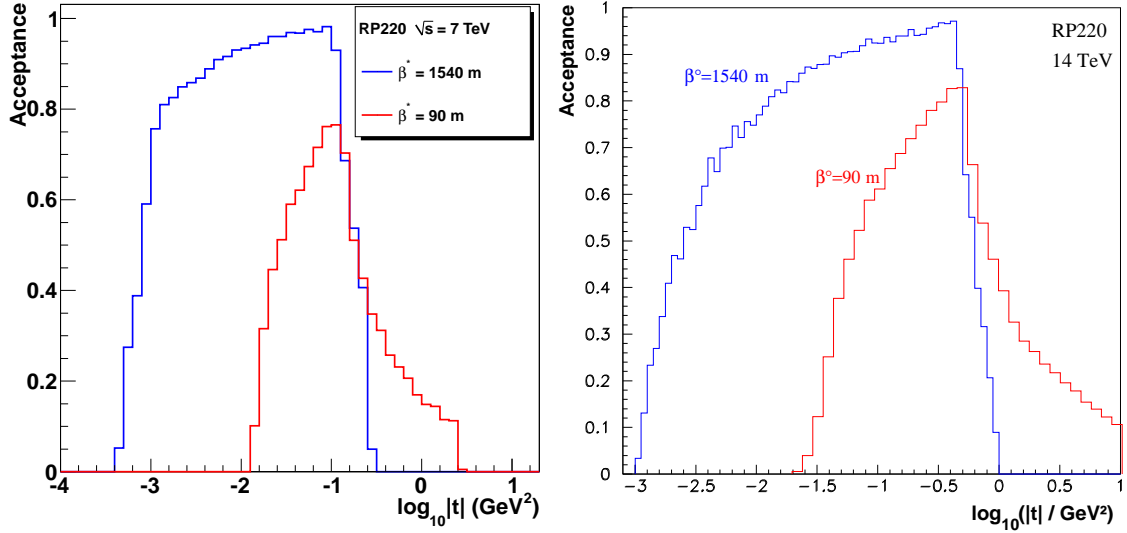


Figure 15: t -Acceptance for $\beta^* = 90 \text{ m}$ and $\beta^* = 1540 \text{ m}$ at $\sqrt{s} = 7 \text{ TeV}$ (left) and 14 TeV (right).

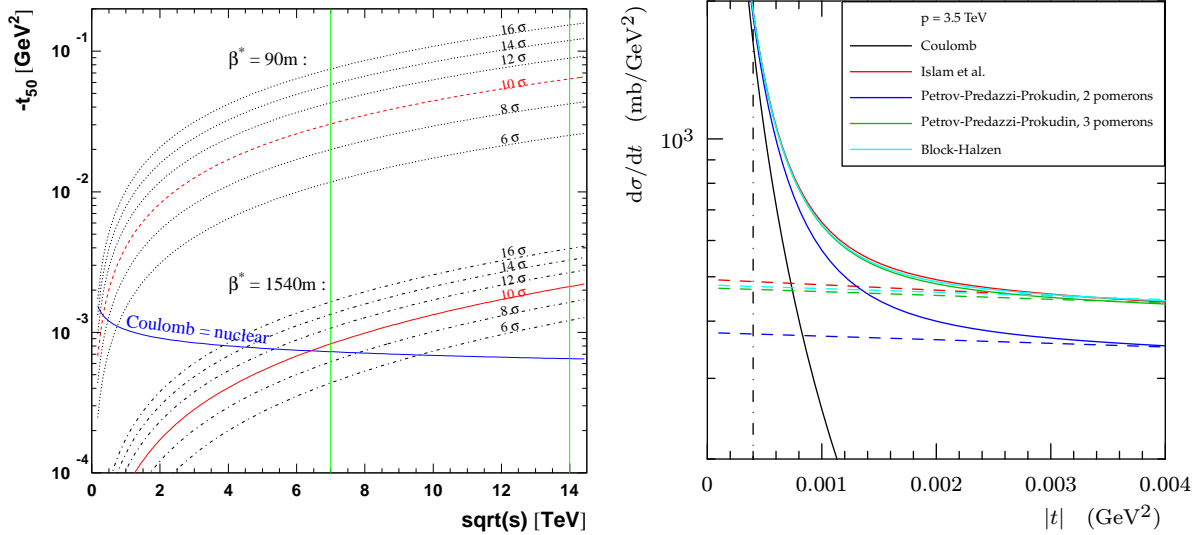


Figure 16: Left: As a function of the centre-of-mass energy \sqrt{s} , the black and red curves indicate the t value at which the RP detector acceptance is 50% if the pot window approaches the beam to a given distance expressed in terms of beam widths σ (curve labels). The active detector surface begins $\delta = 0.5 \text{ mm}$ further away than the window distance shown (due to window thickness and window-detector gap). The t values shown take δ into account. The top group of curves corresponds to $\beta^* = 90 \text{ m}$ with standard emittance $\varepsilon_n = 3.75 \mu\text{m rad}$, the bottom group represents $\beta^* = 1540 \text{ m}$ with reduced emittance $\varepsilon_n = 1 \mu\text{m rad}$. At the blue line, the Coulomb and the nuclear scattering amplitudes have equal moduli. Right: Differential cross-section of elastic scattering at $\sqrt{s} = 7 \text{ TeV}$. Black continuous line: Coulomb component; coloured lines: predictions of various hadronic models [3] for the hadronic component (dashed lines) and the combined cross-section (continuous lines). The minimum $|t|$ accepted at $\beta^* = 1540 \text{ m}$ is represented by the dash-dotted vertical line.

$\frac{1}{\sqrt{\gamma}} \propto \frac{1}{\sqrt{p}}$ dependence of the beam width σ . The resulting effect behaves like

$$|t_{50}| \propto p^2 \left(\frac{C^2}{p} + 2\frac{C\delta}{\sqrt{p}} + \delta^2 \right) = C^2 p + 2C\delta p^{3/2} + \delta^2 p^2. \quad (5)$$

where the definition of the constant C follows from Eqn. (4). The acceptance improvement in terms of t_{min} when reducing \sqrt{s} from 14 TeV to 7 TeV is summarised in Table 3.

β^* [m]	$\sqrt{s} = 7$ TeV:		$\sqrt{s} = 14$ TeV:	
	$ t_{min} $	$ t_{50} $	$ t_{min} $	$ t_{50} $
90	0.012	0.024	0.025	0.05
1540	4×10^{-4}	8×10^{-4}	1×10^{-3}	2×10^{-3}

Table 3: $|t_{min}|$ and $|t_{50}|$ (all in GeV^2) for the $\beta^* = 90$ m and the $\beta^* = 1540$ m optics at the centre-of-mass energies of 7 TeV and 14 TeV.

Comparing the values from Fig. 16 (left) or Table 3 with the differential cross-section curves in Fig. 16 (right) demonstrates that for $\sqrt{s} = 7$ TeV, $\beta^* = 1540$ m and a distance $\leq 10\sigma$ the experiment would become sensitive to the Coulomb component of elastic scattering, which is not reachable with the same optics at 14 TeV.

4.2.2 Extrapolation of the Differential Cross-Section to $t = 0$

The method for extrapolating $d\sigma/dt$ to $t = 0$ at $\sqrt{s} = 7$ TeV will be the same as at 14 TeV, described in Refs. [2, 10], and the uncertainty contributions are expected to be very similar. The key advantage of the lower energy, however, is the about 50% shorter extrapolation interval, which will reduce the fit-induced statistical error and the systematic uncertainty contribution from the model dependence of the extrapolation function. The beam divergence at 7 TeV is higher than at 14 TeV by a factor $\sqrt{14/7} = \sqrt{2}$ (i.e. $3.3 \mu\text{rad}$ instead of $2.4 \mu\text{rad}$, for $\beta^* = 90$ m at both energies), but as explained in [2] (Section 6.3.2), this effect leads to a shift in the extrapolation result which can be corrected for. The optical functions are expected to be known to within 1%, which would translate into an extrapolation uncertainty contribution of 1.5%. Therefore, a total error estimate of $\sim 2\%$ for the extrapolation at $\beta^* = 90$ m and 7 TeV can be considered as conservative.

4.2.3 Commissioning Plan for the $\beta^* = 90$ m Optics

The preparation for TOTEM physics at $\beta^* = 90$ m requires a sequence of Machine Development studies to demonstrate the feasibility of the un-squeeze in β^* from 11 m to 90 m with external tune compensation [11, 12].

The un-squeeze to higher β^* goes in the opposite direction of what is normally done. For the first time, the trim power converters for the triplet will be needed. The powering of the insertion quadrupoles will be much less anti-symmetric than usual and in some cases close to the limits. It could be that inconsistencies in polarities and strength limits are found which may require hardware interventions or redoing optics files. It will be important that the feasibility tests will be done well before the planned physics operation at 90 m. The proposed tests are of general interest for any high-beta option.

Details of the steps to be performed:

1. Full consistent set of optics files for IP5 from 11 m to 90 m in 19 intermediate steps with external tune compensation using the arc quadrupoles. **Done**; for the optics files see [12].
2. Transfer of these files into the control system and global checks using the online model. **Done**.
3. Cold checkout, i.e. driving the magnets based on the optics files without beam. This could be done parasitically in short periods without beam. **Expected to happen soon**.
4. Test at injection energy with beam of the first steps of the un-squeeze. This should allow to spot possible major faults like polarity errors on the triplet trims. From the recent k-modulation measurements it is already known that the extra trim power converters on the triplet work with the correct polarity.
Estimate of the time still needed: 1 hour with low intensity beam at injection + resetting for standard injection.
5. Actual Machine Development:
Beam conditions: End of ramp at 3.5 TeV, 1 bunch per beam, each with about 1×10^{10} protons. Un-squeeze in several steps towards 90 m; in each step perform beta-beating measurements.
Estimate: 1 shift with beam for the feasibility test of the un-squeeze.
Providing collisions at 2×3.5 TeV with low intensity at $\beta^* = 11$ m should be straightforward and not require any optics commissioning time. Stopping the un-squeeze at an intermediate value to do some physics should also be rather straightforward.

4.2.4 Prospects for Very-High β^* Optics at $\sqrt{s} = 7$ TeV

The current version of the $\beta^* = 1540$ m optics for TOTEM is compatible with operation at $\sqrt{s} = 10$ TeV to 14 TeV [11]. At lower energy the two main limiting parameters are the minimum strength allowed in the insertion quadrupoles and the aperture. One way to avoid these limitations would be to loosen the constraints on the phase advance by abandoning the condition to have “parallel to point focussing” in both transverse projections. Investigation on alternative optics at very high β^* , compatible with operations at $\sqrt{s} = 7$ TeV are in progress, in collaboration with the LHC Optics Group.

References

- [1] TOTEM Collaboration: *Technical Design Report*, CERN-LHCC-2004-002; addendum CERN-LHCC-2004-020.
- [2] G. Anelli et al. (TOTEM Collaboration): “The TOTEM Experiment at the CERN Large Hadron Collider”, 2008 JINST 3 S08007.
- [3] V. A. Petrov, E. Predazzi and A. Prokudin: Coulomb interference in high-energy p p and anti-p p scattering, *Eur. Phys. J. C* 28 (2003) pp. 525–533.
M. M. Block, E. M. Gregores, F. Halzen and G. Pancheri: Photon proton and photon photon scattering from nucleon nucleon forward amplitudes, *Phys. Rev. D* 60 (1999) 054024.
M. M. Islam, R. J. Luddy and A. V. Prokudin: Near forward pp elastic scattering at LHC and nucleon structure, *Int. J. Mod. Phys. A* 21 (2006) pp. 1–42.
- [4] S. Giani on behalf of the TOTEM Collaboration:
“TOTEM – Preliminary Physics Results”, LPCC, 6 August 2010,
<http://indico.cern.ch/conferenceOtherViews.py?confId=102669>
- [5] M.G. Ryskin, A.D. Martin and V.A. Khoze, *Eur. Phys. J. C* 54, 199 (2008).
- [6] E. Gotsman, E. Levin, U. Maor and J.S. Miller, TAUP-2878-08; arXiv:0805.2799 [hep-ph] (2008).
- [7] R. Engel, PHOJET program version 1.1X.
- [8] T. Sjöstrand, PYTHIA program version 6.4X.
- [9] T1 Installation EDR agenda:
<http://indico.cern.ch/conferenceDisplay.py?confId=97882>
- [10] TOTEM Collaboration: “Early TOTEM Running with the 90 m Optics”, CERN-LHCC-2007-013 / G-130, March 2007.
- [11] H. Burkhardt, S. White: “High- β^* Optics for the LHC”, LHC Project Note 431, May 2010.
- [12] H. Burkhardt: private communication. The intermediate optics files from $\beta^* = 11$ m to 90 m are available at:
[/afs/cern.ch/eng/lhc/optics/V6.503/HiBeta/un-squeeze-11-to-90m](http://afs/cern.ch/eng/lhc/optics/V6.503/HiBeta/un-squeeze-11-to-90m)